Oxygen Barrier and Mechanical Properties of Masterbatch-Based PA6/Nanoclay Composite Films

Mohammad Fasihi, Mohammad Reza Abolghasemi

Technology of Polymer Research Group, Iranian Academic Center for Education, Culture and Research (ACECR), Branch of Amirkabir University of Technology, Tehran, Iran

Received 15 June 2011; accepted 13 August 2011
DOI 10.1002/app.35467
Published online 17 December 2011 in Wiley Online Library (wileyonlinelibrary.com).

ABSTRACT: This study focuses on the possibility of improving performance properties of polyamide-6 (PA6) nanocomposite films for packaging application using nanoclay masterbatch. Different concentrations of nanoclay in PA6 were prepared through melt-mixing of particulate nanoclay and nanoclay masterbatches in a twin screw compounder, then film samples were molded using a hot press. Oxygen barrier properties were then measured and interpreted on the basis of different theoretical approaches. Also, a correlation between morphology and properties of the studied nanocomposites was observed, and all prepared nanocomposites exhibited performance improvement with increasing the nanoclay content. The masterbatch-based nanocomposite films showed more exfoliated regions that leading to the enhancement of the mechanical properties. Gas permeability through nanocomposite films decreased significantly just by loading a small amount of nanoclay. However, surprising behavior in oxygen permeability observed at higher levels of nanoclay in masterbatch-based nanocomposite was attributed to the decreased crystallinity of PA6 matrix. © 2011 Wiley Periodicals, Inc. J Appl Polym Sci 125: E2–E8, 2012

Key words: barrier; nanocomposites; polyamides; TEM; films

INTRODUCTION

Over the last decades, a great deal of researches have been devoted to the different aspects of polymer-layered silicate nanocomposites that have shown promising improvements in mechanical properties, permeability, thermal stability, and flame retardency, especially, at low nanofiller volume fraction.[1–3] These enhancements are achieved without impairing the optical clarity and density of the polymer matrix, and depend on such factors as aspect ratio of the filler, degree of dispersion, and the strength of the interparticle interactions.[4,5]

One of the most interesting applications of polymer-layered silicate nanocomposites is the field of packaging. In this application, the reduction of oxygen permeability is of crucial importance to the prevention from food spoilage. Although the enhancement in gas barrier properties is well-known in polymer-silicate nanocomposites, it depends on various factors such as the relative orientation of the nanoclay layers in the matrix and the state of aggregation and dispersion, that is, intercalation or exfoliation.

Correspondence to: M. Fasihi (mfasihi@aut.ac.ir).
Contract grant sponsor: Iranian Academic Center for Education, Culture and Research (ACECR).

Substantial industrial and scientific researches have been focused on polyamide-based nanocomposites prepared via melt compounding due to the polarity, low price, availability, and wide use of polyamides in packaging applications. Hydrophilic nature of polyamides is favorable for a good compatibility with silicates.[5–7] In addition, melt processing technique is particularly interesting owing to its good affinity with the existent processes used in commercial applications.

Various studies have been reported on the relationship between the microscopic structure of nanocomposites and their gas transport properties. Incorporating layered silicate into the polymeric matrix improves its gas barrier properties, mainly by reducing the volume available for gas transport as well as providing a more tortuous path for penetrant molecules. Nanoclay platelets with a higher aspect ratio expectedly must lead to a more tortuous path for diffusion path. A simple relationship between filler volume fraction and relative permeability of polymer composites derived by Nielson and improved by following works.[8–10] According to these models, relative permeability decreases monotonically with the increase of filler content, and that can be correlated to the filler volume fraction, Aspect ratio, orientation of nanoclay platelets in the polymeric matrix and the state of aggregation and dispersion.[8–10] Also, some physicochemical factors, such as glass transition temperature, mean free volume of polymer, and the solubility of the penetrant gas in polymer, influence the permeability of polymeric

matrix.[11] Incorporation of nanoclay would change some polymeric matrix behavior, for example, chain rigidity or intersegmental distance, that would cause deviation of the gas permeability of the nanocomposites from proposed models.

However, gas barrier properties of polyamide nanocomposite films prepared by melt compounding have not been completely investigated. Several numbers of formulation and processing factors affect the achievement of exfoliated silicate structure, as the main controlling parameter of final properties of nanocomposite.[12–14] In this study, oxygen permeability and mechanical properties of polyamide-6 (PA6)/layered silicate nanocomposite films were examined using particulate nanoclay and nanoclay masterbatch and correlated to the nanostructure of produced films through different techniques. Furthermore, the permeability data have also been compared with the theoretical models to predict barrier enhancement.

EXPERIMENTS

Materials

Modified sodium montmorillionite clay nanofill SE3010, and two masterbatches Ma3010 and Mb3010, were supplied by Sud-Chemie AG. Ma3010 contained 50 wt % PA6, and Mb3010 contained 50 wt % amorphous polyamide, whereas both contained 50 wt % Nanofill SE3010. Nanofill SE3010 is an alkyl ammonium treated powder with an average particle size of 8 μm. Extrusion grade of PA6 was provided from DSM engineering plastics (Akulon F130-B) with melt flow index = 0.7 g/10 min which is suitable for film packaging application.

Sample preparation

Melt blended PA6 and nanoclay were prepared using a ZSK25 twin screw extruder ($L/D = 40$) equipped with vacuum venting. The barrel temperature profile of 230, 235, 240, 250, and 260°C from feeding to die zone, and screw speed of 400 rpm were adjusted. The extrudates were granulized when they got out of the pelletizer. Nanocomposite granules with nominal nanoclay content of 3, 5, and 7 wt % nanoclay were prepared according to the method mentioned earlier. Each of the masterbatches was diluted with PA6 using the same processing conditions to produce nanocomposites with the stated nanoclay concentration.

Thin films of the nanocomposites were prepared by compression molding at 240°C and pressure of 30 bars. The film samples were then cooled down and used for tensile and gas permeation measurements. True percent of nanoclay in all samples was determined by measuring the ash content of nanoclay and film samples in a hot furnace at 600°C. Nanoclay showed almost 35 wt % weight loss that should be related to the surface modifier used in nanoclay treatment. The formulation of samples is presented in Table I. Pure PA6 film, as the control sample, was also prepared under similar conditions.

TABLE I
The Composition of Nanocomposite Samples and Pure PA6 Control

System	Nanoclay types	Nominal mineral (wt %)	Measured mineral (wt %)
PA	–	0	0
PA/SE3	SE3010	3	3.12
PA/SE5	SE3010	5	5.05
PA/SE7	SE3010	7	7.11
PA/Ma3	Ma3010	3	2.94
PA/Ma5	Ma3010	5	4.92
PA/Ma7	Ma3010	7	6.84
PA/Mb3	Mb3010	3	2.89
PA/Mb5	Mb3010	5	4.87
PA/Mb7	Mb3010	7	6.77

Characterization methods

Tensile tests were performed in accordance with ASTM D882 at room temperature and relative humidity (RH) of 45% using an Instron instrument equipped with a 1 kN load cell at a crosshead speed of 50 mm/min. The thickness of samples was about 150 μm. For each nanocomposite sample, the average of at least five measurements was reported.

Oxygen transport within the films was determined with GPC-D Munchen permeability device at 25°C and RH values of 50% according to ASTM D1434 standard method. The equipment consists of two chambers between which the film is placed. The machine, records the increasing of oxygen pressure, P, as a function of the time, t. From pressure-time curve, the software calculates permeation that can be converted to permeability knowing the film thickness. The diffusion coefficient, D, can then be calculated by the following equation:[15]

$$D = L^2/6\tau \quad (1)$$

where L is the thickness of the film and τ is the time lag, obtained from pressure-time plot provided by the software.

X-ray diffractometer (XRD) patterns for the prepared samples were recorded on a Phillips X'Pert diffractometer at a scan rate of 1.0°/min within the scattering angle range 2θ from 1 to 30° using standard nickel filter. X-ray radiation characterized by a wavelength of 1.54 Å. The diffractometer operated at a voltage of 40 kV and a current of 40 mA.

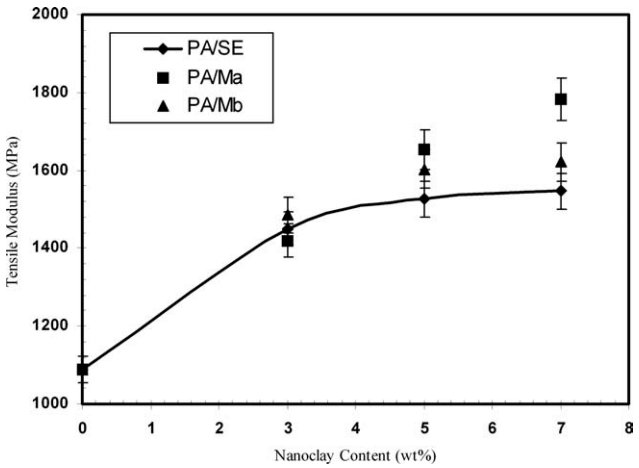

Figure 1 Comparison of tensile modulus of nanocomposite films prepared from nanoclay SE3010, Ma3010, and Mb3010, at different nanoclay loading.

The layer morphology of nanocomposites was examined by transmission electron microscope (TEM) using FEG PHILIPS model.

A differential scanning calorimeter, DSC1 MEETTLER TOLEDO, was used to measure thermal transitions and crystallinity at a heating rate of 20°C/min, under nitrogen gas. Crystallinity of the samples was calculated from $\Delta H_m/207.1$ ratio, where ΔH_m and 207.1 are enthalpy of melting for partial and 100% crystallinity both in j/g, respectively.

RESULTS AND DISCUSSION

The mechanical performance of the PA6 nanocomposites was studied by tensile measurements at room temperature. Figure 1 shows the tangent tensile modulus (elastic modulus) of the prepared nanocomposites as a function of organoclay content. As shown, tensile modulus of nanocomposite with 5 wt % loading of organoclay (PA/SE5) was increased about 40% compared to neat PA6, which is in good agreement with other research works.[16–18] Beyond this concentration, there was a slight increase in tensile modulus of PA/SE7, whereas modulus of PA/Ma7 increased considerably (around 60%) relative to neat PA6. Masterbatch-based nanocomposites showed more linear behavior and higher tensile modulus, which suggested the better silicate dispersion in these samples compared to PA/SE nanocomposites.

Figure 2 represents the tensile strength of nanocomposite films as a function of nanoclay concentration. The addition of the organoclay leads to a substantial improvement in the tensile strength of different nanocomposites. Compared to pure PA6, samples of PA/Ma5 and PA/Mb5 exhibited 25 and 20% increase in tensile strengths, respectively. Improvement in tensile strengths of nanocomposite films might be attributed to the good compatibility between treated nanoclay and polyamide.

XRD and TEM are complementary techniques in examining the structure and morphology of polymer nanocomposites. Figure 3 illustrates the XRD scans of nanocomposite films. The *d*-spacing, which is defined as a bulk sum of layer thickness and interlayer distance, can be calculated by Bragg's law. The XRD spectra for nanoclays SE3010 and Ma3010 exhibited strong reflections at low $2\theta \sim 2.5$, 4.6, and 7.2° corresponding to *d*-spacings of 35, 19, and 12 Å, respectively. A shift to lower angles of characteristic diffraction peak suggested an increase in interlayer spacing of galleries of clay, which is referred to as intercalation. Disappearance of the diffraction peak indicated possible exfoliation of the clay platelets. XRD results of specimen PA/SE3 showed flat diffraction profile and the absence of any basal reflections indicating that the ordered layers of nanoclays in the nanocomposites have been disrupted. It meant that this sample should have a good degree of exfoliation. Other specimens showed weak reflection in smaller angle (larger *d*-spacing) about 2.5° (*d*-spacing = 35 Å). Also, PA/SE7 showed a peak at 4.9° corresponding to *d*-spacing of 18 Å. These reflections could indicate the existence of partially intercalated morphology in these samples.

Figure 3 shows the other diffraction peaks at 2θ angle of 19–24°, which would be a *d*-spacing of about 4.7–3.7 Å, and are attributed to the crystalline structure of polyamide matrix. Polyamides can display two major crystal forms: the α-phase that is, thermodynamically the more stable, and the γ-phase, obtains at nonisothermal crystallization conditions, especially, for rapid cooling such as at the surface of molded samples. The α and γ-crystalline forms were identified by peak intensities occurring at ~ 23.7° for the α-form, and 21.3° for the γ-form. It is well-known that the addition of nanoclay can change the degree of crystallinity by acting as a nucleant, as well as causing different crystal structures.[19–22]

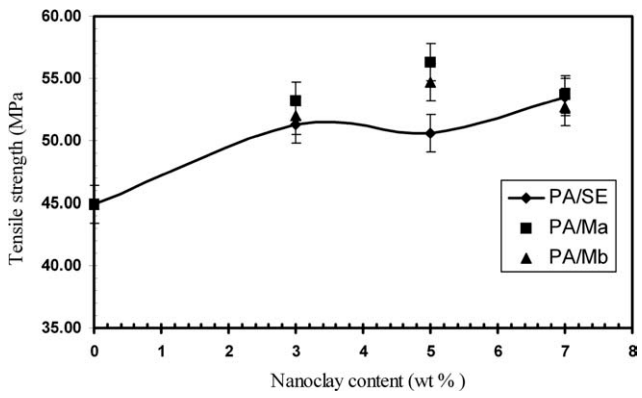

Figure 2 Tensile strength of nanocomposite films containing different nanoclay loading.

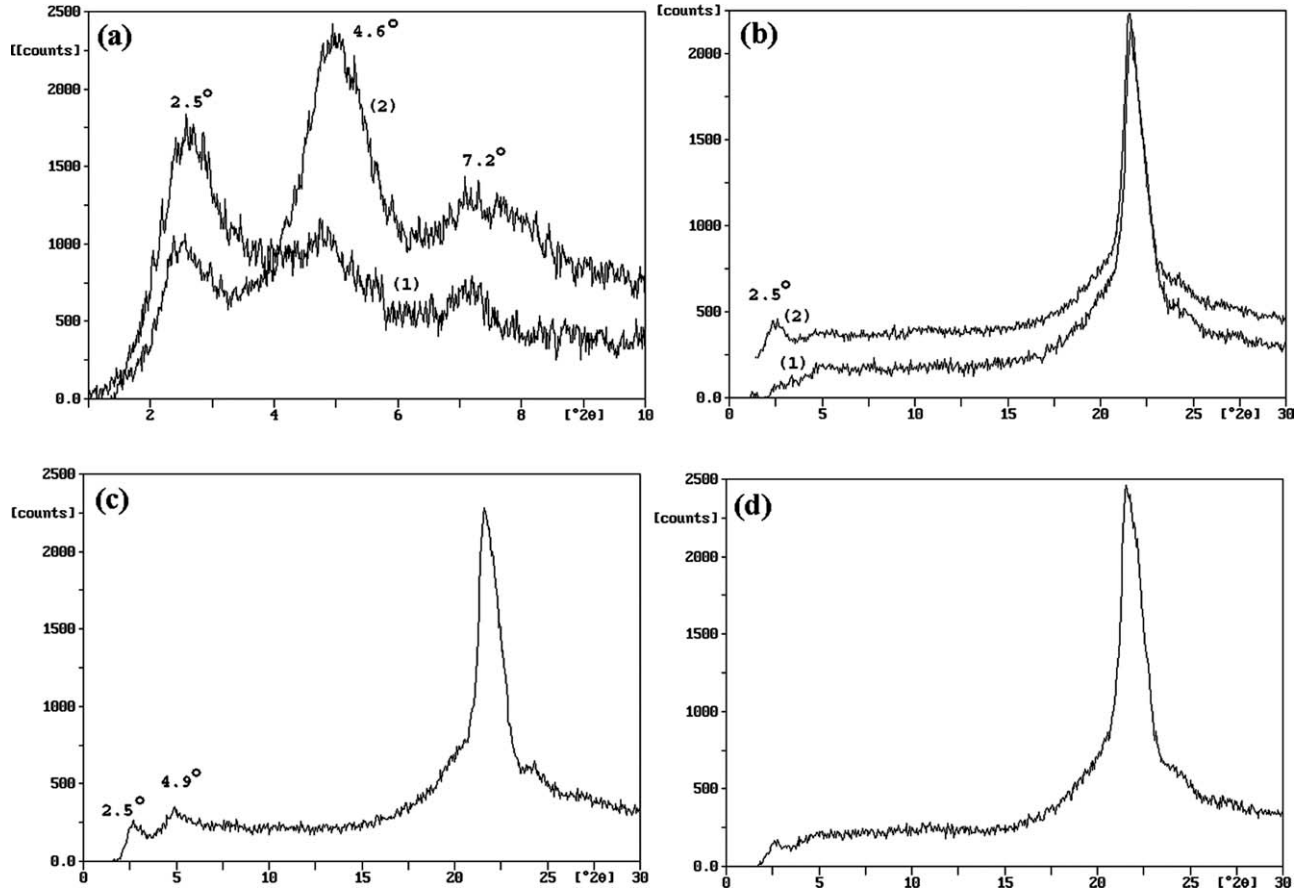

Figure 3 XRD scans for specimens (a-1) SE3010, (a-2) Ma3010, (b-1) PA/SE3, (b-2) PA/SE5, (c) PA/SE7, and (d) PA/Ma5.

Although XRD scans suggested only a low degree of intercalation, the morphology observed with TEM (Figs. 4 and 5) indicated the presence of both intercalated and exfoliated structures. Therefore, XRD results must be verified with TEM micrographs. The general impression obtained from TEM was that the use of masterbatch builds up a higher degree of exfoliation that confirms the better mechanical properties of masterbatch-based nanocomposites. The maximum aspect ratio of the layers as deduced from the TEM micrographs was about 210 in all samples.

Figure 5(a) illustrates TEM micrograph of PA/SE5, from which it is obvious that different degrees of intercalation are presented in the vicinity of exfoliated layers. It can also be seen that the single layers and some intercalated stacks of few layers are bent and folded. The general idea is that masterbatch-based nanocomposites render more exfoliated layers than intercalated tactoids. Although the XRD scan of the composites of all three forms of filler looked similar, we got the impression from TEM micrographs of PA/Ma5 and PA/Mb5 nanocomposites (containing 5 wt % of nanoclay Ma3010 and Mb3010) that these masterbatches gave more exfoliated layers than particulate nanoclay.

Oxygen permeation of nanocomposite films was measured by the determination of the amount of oxygen passing through the parallel surfaces of samples in unit time according to the procedure described in the Experimental Section. Table II reports the oxygen permeability (P) and diffusivity (D) of nanocomposite films at different nanoclay contents. As it is obvious, permeability and diffusivity values of films decreased to lower amount in the same manner, by the increase in nanoclay loading. Oxygen permeability was reduced by a factor of four over the pure polyamide by incorporation of 3 wt % nanoclay. As the nanoclay loading was increased to 7 wt %, only a slight improvement in permeation resistance was observed. Oxygen transport of masterbatch-based nanocomposites was a little higher compared to nanocomposites obtained from SE3010. Also, some increase in relative permeability was observed in PA/Mb7 compared to PA/Mb5. This behavior have been reported by several researchers such as Osman et al. in the PU-nanoclay composite film, Frounchi and coworkers in the low-density polyethylene/linier low-density polyethylene/organoclay nanocomposite films and Suter and coworkers in the epoxy/nanoclay composite

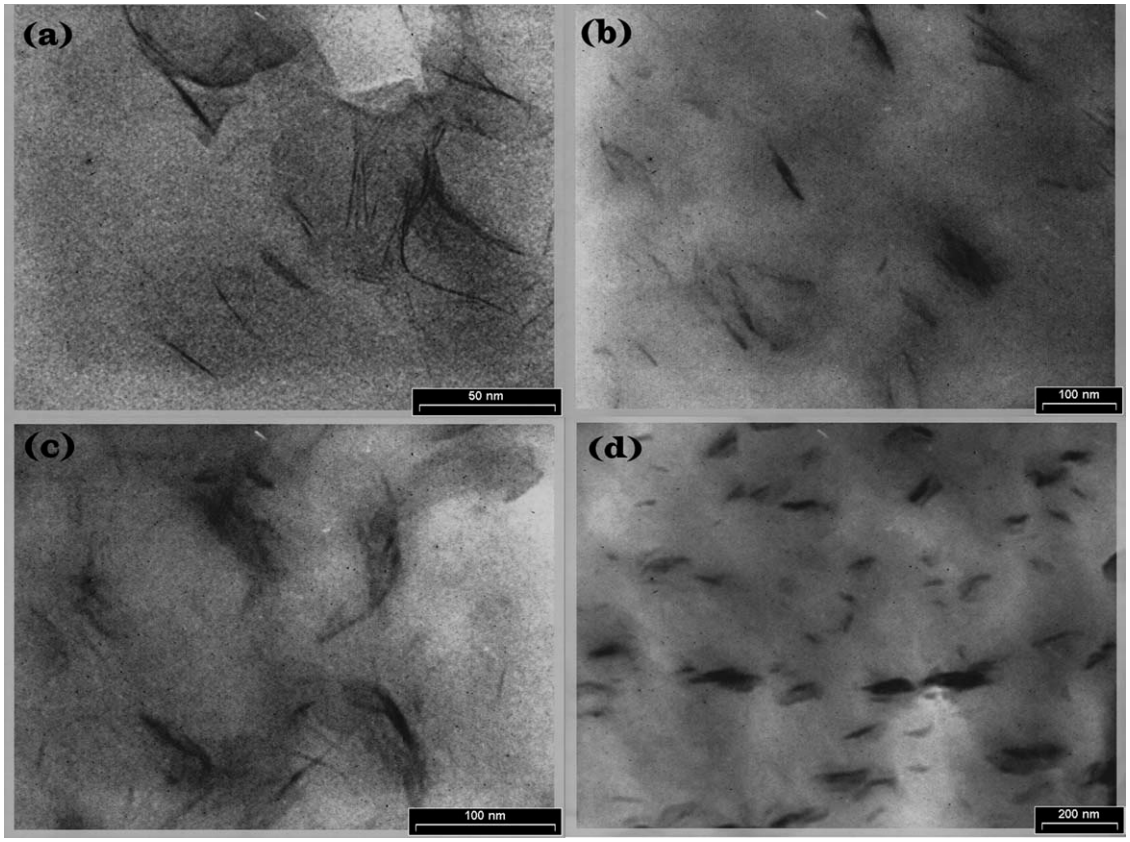

Figure 4 TEM micrographs of (a and b) PA/SE3, (c) PA/SE5, and (d) PA/SE7.

systems.[23–25] In nonpolar hydrocarbon treated filler and semipolar matrix system, the change in the morphology as a result of phase separation at the interface between filler coating and matrix, leads to a decrease in the density of the organic material or higher free volume at the interface and, therefore, increase in the permeation rate through the composite film.[23] Also, the decrease in aspect ratio of nanoclay in nanocomposites with higher filler contents during melt processing can cause the permeability of nanocomposites to increase.[24] Suter and coworkers stated that the intercalated part of the filler did not contribute much to the permeability reduction and that the exfoliated layers were those which built the permeation barrier. Thus, the lower degrees of exfoliation, the higher the gas transport properties.[25]

The increase in oxygen transmission rate in PA/Mb7 should be correlated to the existence of amorphous polyamide in Mb3010 masterbatch, as it was the only difference with other composites. It can only influence the gas solubility in the composite moderately, which cannot be expected to cause to the observed reverse trend. Crystalline lamellae of matrix are impermeable to small molecules and are then likely to induce tortuosity effects toward the diffusing penetrant, similar to nanoclay sheets. Differential scanning calorimetry (DSC) was used to characterize the crystalline nature of the polyamide matrix in these nanocomposites. Although the XRD scans showed the superiority of the γ-crystal form, DSC results showed the existence of both crystal types even at thickness of 150 μm of the films. Figure 6 shows DSC melting endotherms of nanocomposite films. First, low temperature endothermic peaks around 210°C were introduced with the addition of clay, which was related to γ-form crystals. Second, the main endotherm peak around 220°C which was recognized as the α-form crystals. Introducing the clay to PA6 increased γ-form crystal fraction significantly, whereas total crystallinity changed a little. Table III summarizes data collected from such scans. As shown, the lowest crystallinity was obtained in the case of PA/Mb7 which showed the highest permeability. It was assumed that a reduction in crystalline lamellae can neutralize the addition of nanoclay in improving the gas permeability of PA6/nanoclay composites.

Several studies on modeling the barrier properties of polymer nanocomposites have been performed based on the tortuous pathway concept, wherein, the functionalized gas barrier properties are assumed to be dependent on parameters such as particle size of layered silicate, relative orientation, and the state of aggregation and dispersion (intercalation, exfoliation, or partially exfoliation). Layered

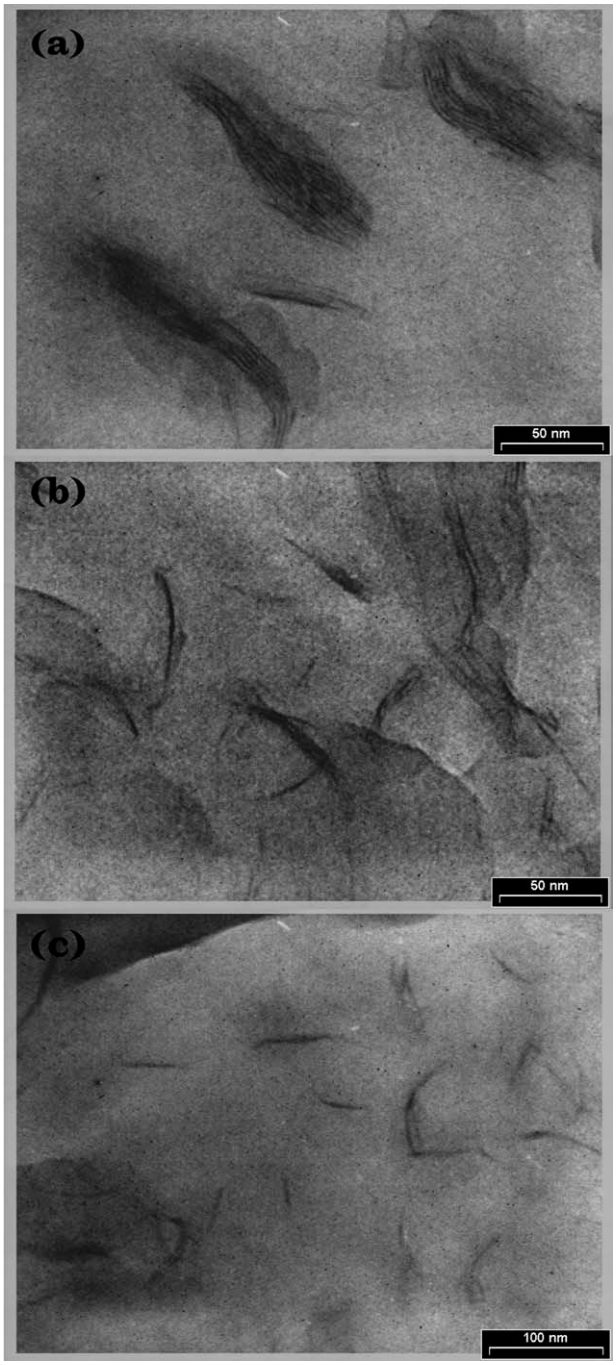

Figure 5 TEM images of specimens (a) PA/SE5, (b) PA/Ma5, and (c) PA/Mb5.

morphology of nanoclay is particularly effective at maximizing the length of penetration in the presence of filler. At first, Nielsen performed modeling of the barrier properties of polymer composites containing oriented and regularly arrayed flakes based on a tortuous pathway concept.[8] Cussler and coworkers[26] then conducted systematic studies and proposed new models to take additional factors into account, including the shape, dimension polydispersity, and array of the dispersed nanoplatelets. The diffusion

TABLE II
Oxygen Permeability and Diffusion Coefficient Data for all Sample Films

System	Mineral volume fraction	Permeability, P (cm^3 mm)/(m^2 day bar)	Diffusivity, D (cm^2/s)
PA	0	1.41	15.8
PA/SE3	1.21	0.38	5.2
PA/SE5	2.04	0.33	4.6
PA/SE7	2.89	0.30	4.3
PA/Ma3	1.21	0.41	5.3
PA/Ma5	2.04	0.33	5.2
PA/Ma7	2.89	0.34	5.2
PA/Mb3	1.21	0.40	5.1
PA/Mb5	2.04	0.39	5.4
PA/Mb7	2.89	0.49	6.3

in nanocomposites containing oriented, randomly arrayed disks parallel to the surface of the nanocomposite films was also modeled by Fredrickson and Bicerano[27] and Gusev and Lusti.[28] Bharadwaj improved Nielsen's model by simply introducing a new order parameter as the following:[10]

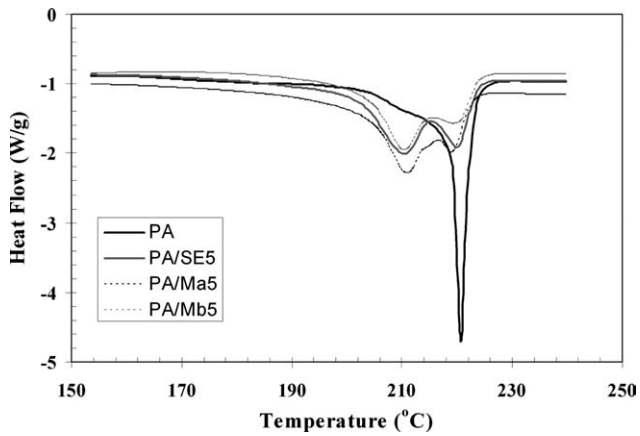

Figure 6 DSC curve of PA6 and nanocomposite films.

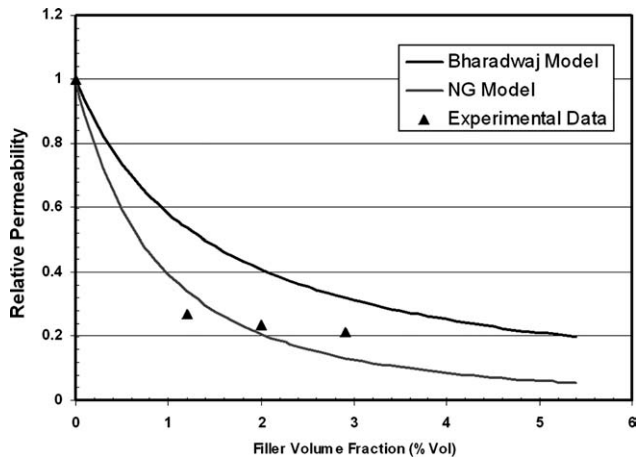

Figure 7 Experimental permeability data of PA/SE against silicate volume fraction compared with Bharadwaj and NG models.

TABLE III
Crystallinity Percent Measured by DSC Technique

System	Crystallization percent
PA	25.2
PA/SE5	27.7
PA/SE7	28.9
PA/Ma5	28.1
PA/Ma7	26.4
PA/Mb5	26.7
PA/Mb7	22.2

$$\frac{P_o}{P_f} = \frac{1-\varphi}{1+\frac{L}{2w}\varphi(2/3)(S+0.5)} \quad (2)$$

where P_o and P_f represent the permeabilities of nanocomposite and pure polymer, respectively. φ, L, w, and S show the volume percentage of the nanoclay, length, width, and the order parameter that includes the orientational order and can be defined as:

$$S = \frac{1}{2} < 3\ \cos^2(\theta) - 1 > \quad (3)$$

where θ represents the angle between the direction of preferred orientation and the sheet clay normal unit vectors. Another model called NG model was developed by Ghasemi et al.[29] based on the Cussler-Lape idea which took the distribution of layers orientation into consideration. The relative permeability of nanocomposite film was formulated by idealizing a clay-filled film with a random array flakes and measuring the effective permeability by the product of reduced area and the increased path length. The average distance traveled per flake was determined by assuming that the solute hits the flake at a random point along its length. According to this assumption, relative permeability was given by:[29]

$$\frac{P_o}{P_f} = \frac{1-\varphi}{\left[1+\frac{\alpha\varphi}{3}\left(\frac{\sum_j n_j(\cos\theta_j)^2}{\sum_j n_j \cos\theta_j}\right)\right]^2} \quad (4)$$

where n_j is the number of flakes with direction angle θ_j. This angel represents the angle between the direction of preferred orientation and the platelet normal vector. The relative permeabilities of nanocomposite samples with different volume fractions of fillers were compared with those predicted by NG as well as Bharadwaj models. As can be observed in Figure 7, the NG model fits the experimental data much better than the Bharadwaj model. This could be attributed to the fact that in the Bharadwaj model, the orientation distribution of silicate layers is not considered.[29]

CONCLUSION

In this work, nanocomposite PA6 films at different nanoclay loadings were prepared using nanoclay masterbatch and particulate nanoclay. Masterbatch-based nanocomposite films showed more improvements in mechanical properties and similar oxygen permeation. In particular, nanocomposite films based on Ma3010 exhibited the best performances. XRD scans and TEM micrographs collectively demonstrated the good dispersion and orientation of silicate platelets inside the matrix, as well as the possible presence of polymer–clay interactions. TEM images suggested higher fractions of well-exfoliated silicate platelets and a more pronounced orientation of the layers within masterbatch-based nanocomposites. Also, the experimentally measured permeability data were interpolated on the basis of different theoretical approaches and new NG model. Using the aspect ratio and order parameter from TEM images, the new NG model fitted the experimental data better than the Bharadwaj model.

References

1. Ke, Y.; Long, C.; Qi, Z. J Appl Polym Sci 1999, 71, 1139.
2. Becker, O.; Cheng, Y.; Varley, J. R.; Simon, G. P. Macromolecules 2003, 36, 1616.
3. Alexandre, M.; Dubois, P. Mater Sci Eng 2000, 28, 1.
4. Ray, S. S.; Okamoto, M. Prog Polym Sci 2003, 28, 1539.
5. Pinnavaia, T. J.; Beall, G. W., Eds. Polymer-Layered Silicate Nanocomposites; Wiley: New York, 2001.
6. Lebaron, P. C.; Wang, Z.; Pinnavaia, T. J. Appl Clay Sci 1999, 15, 11.
7. Maiti, P.; Okamoto, M. Macromol Mater Eng 2003, 288, 440.
8. Yamamoto, H.; Mi, Y.; Stern, S. A. J Polym Sci Part B: Polym Phys 1990, 28, 2291.
9. Fornes, T. D.; Paul, D. R. Polymer 2003, 44, 4993.
10. Liu, L.; Qi, Z.; Zhu, X. J Appl Polym Sci 1999, 71, 1133.
11. Liu, X.; Wu, Q. Macromol Mater Eng 2002, 287, 180.
12. Nielsen, L. J. Macromol Sci Chem 1967, A1, 929.
13. Cussler, E.; Hughes, S.; Ward, W. J.; Aris, R. J Membr Sci 1988, 38, 161.
14. Bharadwaj, R. Macromolecules 2001, 34, 9189.
15. Comyn, J. Polymer Permeability; Elsevier Applied Science Publishers: New York, 1988.
16. Fornes, T. D.; Yoona, P. J.; Hunterb, D. L.; Keskkulaa, H.; Paula, D. R. Polymer 2002, 43, 5915.
17. Cho, J. W.; Paul, D. R. Polymer 2001, 42, 1083.
18. Fornes, T. D.; Paul, D. R. Polymer 2003, 44, 4993.
19. Wu, Z.; Zhou, C.; Zhou, N. Polym Testing 2002, 21, 479.
20. Liu, X.; Wu, Q.; Berglund, L. A.; Qi, Z. Macromol Mater Eng 2002, 287, 515.
21. Kyotani, M.; Mitsuhashi, S. J Polym Sci Part A 1972, 10, 1497.
22. Fornes, T. D.; Paul, D. R. Polymer 2003, 44, 3945.
23. Dadbin, S.; Noferesti, M.; Frounchi, M. Macromol Symp 2008, 274, 22.
24. Osman, M. A.; Mittal, V.; Morbidelli, M.; Suter, U. W. Macromolecules, 2004, 37, 7250.
25. Osman, M. A.; Mittal, V.; Morbidelli, M.; Suter, U. W. Macromolecules 2003, 36, 9851.
26. Yang, Ch.; Smyrl, W. H.; Cussler, E. L. J Membr Sci 2004, 231, 1.
27. Fredrickson, G. H.; Bicerano, J. J Chem Phys 1999, 110, 2181.
28. Gusev, A.; Lusti, H. R. Adv Mater 2001, 13, 1641.
29. Ghasemi, E.; Navarchian, A. H. Modeling the effects of silicate layer orientation on barrier properties of polymer/clay nanocomposites. In: Proceedings of the 9th International Seminar on Polymer Science and Technology (ISPST), Tehran, October 2009; p 56.